Experimental Demonstration of the Impact of the Parameters of Floating Guard Ring on Planar InP/InGaAs-Based Avalanche Photodiodes' Performance and Its Optimization

Junyang Zhang, Xuanzhang Li, Chunhua Du, Yang Jiang, Ziguang Ma, Hong Chen, Haiqiang Jia, Wenxin Wang, and Zhen Deng

***Abstract*—Suppression pre-breakdown in planar separated absorption, grading, charge and multiplication (SAGCM) avalanche photodiodes (APDs) with the help of Floating Guard Ring (FGR) is still a research hotspot. In this paper, a lattice-matched InP/InGaAs-based SAGCM structure is grown by Metal-Organic Chemical Vapor Deposition and thus the planar 50 μm photosensitive area APDs with different FGR structures are fabricated using zinc diffusion process. The effects of the different lengths of FGR (4 μm, 8 μm, 12 μm, 16 μm), and the different distances between FGR and the Zn diffused p+ region (4 μm, 6 μm, 8 μm, 10 μm) on the optoelectrical characteristics are deeply studied. The results from optical microscope, scanning electron microscope and current-voltage curves reveal that there is an optimal length and distance for the punch-through and breakdown voltage. Furthermore, the nA-level dark current, gain (M) of up to 10 at breakdown voltage, responsibility as high as 9.01 A/W at $M = 10$ and quantum efficiency equaling to 72% are also tested and calculated, proving the good performance of our devices. The optimized FGR parameters and related structure are expected to be helpful for obtaining high-performance, small-size InP/InGaAs-based APDs.**

***Index Terms*—Planar InP/InGaAs-based SAGCM APDs, FGR, punch-through, breakdown.**

Manuscript received 17 February 2022; accepted 20 February 2022. Date of publication 23 February 2022; date of current version 17 March 2022. This work was supported in part by the National Natural Science Foundation of China under Grants 62004218 and 61991441, in part by the Youth Innovation Promotion Association, Chinese Academy of Sciences under Grant 2021005, in part by the Strategic Priority Research Program of Chinese Academy of Sciences under Grant XDB01000000, and in part by the Center for Clean Energy, Institute of Physics, Chinese Academy of Sciences. *(Corresponding author: Zhen Deng.)*

Junyang Zhang and Xuanzhang Li are with the Key Laboratory for Renewable Energy, Beijing Key Laboratory for New Energy Materials and Devices, Beijing National Laboratory for Condensed Matter Physics, Institute of Physics, Chinese Academy of Sciences, Beijing 100190, China, with the University of Chinese Academy of Sciences, Beijing 100049, China, and also with the Center of Materials and Optoelectronics Engineering, University of Chinese Academy of Sciences, Beijing 100049, China (e-mail: zhangjunyang@iphy.ac.cn; lixuanzhang16@mails.ucas.ac.cn).

Chunhua Du and Zhen Deng are with the Key Laboratory for Renewable Energy, Beijing Key Laboratory for New Energy Materials and Devices, Beijing National Laboratory for Condensed Matter Physics, Institute of Physics, Chinese Academy of Sciences, Beijing 100190, China, with the Center of Materials and Optoelectronics Engineering, University of Chinese Academy of Sciences, Beijing 100049, China, and also with the Yangtze River Delta Physics Research Center, Liyang, Jiangsu 213000, China (e-mail: duchunhua@iphy.ac.cn; zhen.deng@iphy.ac.cn).

Yang Jiang and Ziguang Ma are with the Key Laboratory for Renewable Energy, Beijing Key Laboratory for New Energy Materials and Devices, Beijing National Laboratory for Condensed Matter Physics, Institute of Physics, Chinese Academy of Sciences, Beijing 100190, China, and also with the Center of Materials and Optoelectronics Engineering, University of Chinese Academy of Sciences, Beijing 100049, China (e-mail: jiangyang@iphy.ac.cn; zgma@iphy.ac.cn).

Hong Chen, Haiqiang Jia, and Wenxin Wang are with the Key Laboratory for Renewable Energy, Beijing Key Laboratory for New Energy Materials and Devices, Beijing National Laboratory for Condensed Matter Physics, Institute of Physics, Chinese Academy of Sciences, Beijing 100190, China, with the Center of Materials and Optoelectronics Engineering, University of Chinese Academy of Sciences, Beijing 100049, China, and also with the Songshan Lake Materials Laboratory, Dongguan, Guangdong 523808, China (e-mail: hchen@iphy.ac.cn; mbe2@iphy.ac.cn; wxwang@iphy.ac.cn).

Digital Object Identifier 10.1109/JPHOT.2022.3153649

I. Introduction

Boosting interests have been attracted to the research of avalanche photodiodes (APDs). APDs are a kind of detectors, which can transfer photons to electrons and multiply electrons to achieve gains in reverse voltage. Compared to PIN photodetectors, APDs have internal gain, higher sensitivity and higher bandwidth [1]–[3], and thus they have been widely used in many fields, such as lidar, sensing weak optical signal, imaging, single-photon counting and so on [4]–[7]. One of the important branches of APDs is InP/InGaAs-based APDs, which can offer high performance in the range of 0.9–1.6 μm wavelengths (especially in the two important communication band-1310 nm and 1550 nm) [8], [9].

At first, the InP/InGaAs-based APDs utilize the separated absorption and multiplication (SAM) structure [10]–[12]. Unfortunately, SAM APDs have slow speed of response, which is limited by the charge (mainly for holes) accumulation between the InGaAs/InP heterointerface due to the big valence-band discontinuity [13]. Therefore, to suppress above shortage, InGaAsP grading layers are introduced to be sandwiched between InP and InGaAs. Furthermore, to improve the gain-bandwidth product, a thin charge InP layer with high carrier concentrations is inserted between the InP absorption layer and the InGaAsP grading layers. Due to the advantages of high responsivity, high speed and high gain-bandwidth products, many studies of the structure designs (including the concentration and thickness of each layer, comparison between the planar and the mesa structure), the epitaxial growth (the quality of the interface improvement) and the device fabrication have been deeply studied. Nowadays, the

This work is licensed under a Creative Commons Attribution 4.0 License. For more information, see https://creativecommons.org/licenses/by/4.0/

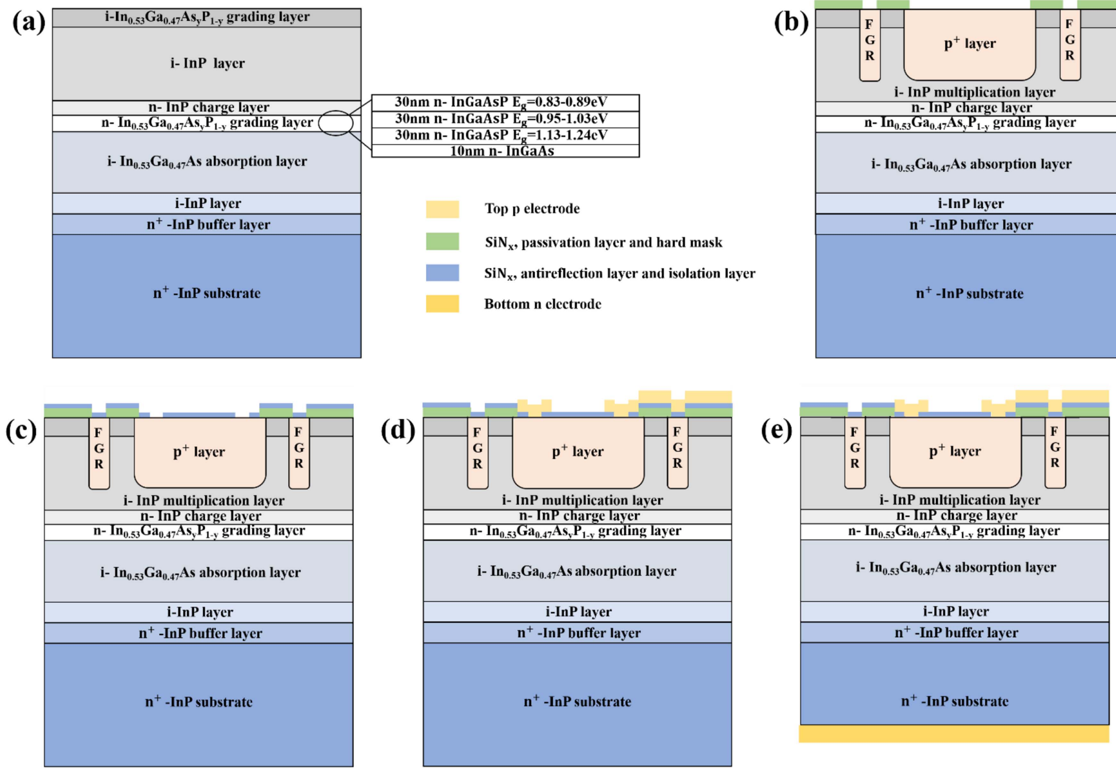

Fig. 1. The cross section of the epitaxial structure and the process flow diagram of the planar InP/InGaAs-based SAGCM APD. (a) The epitaxial structure, and the insert schematic is the specific formation of grading layer, which consists of three band-gap grading InGaAsP layers and one InGaAs layer; (b) the SiN_x hard mask deposition process by ICP-PECVD, the diffusion trench openings process for diffusion regions by RIE and the single zinc diffusion process by MOCVD to form a heavily doped p+ region and FGR; (c) the SiN_x antireflection and isolation layer deposition process by ICP-PECVD and the top p electrode trench opening process for ohmic contact by RIE; (d) the deposition process of top p electrode and p electrode pad by EBE; (e) the back surface's grinding and polishing process, and the deposition process of bottom n electrode.

planar InP/InGaAs-based SAGCM APDs are the mainstream in commercial APDs due to its suppression of surface leakage current efficiently in comparison with the mesa structure [14].

For the planar technical roadmap, the diffusion process to form a p+ region is an important step. After the diffusion process, the edge of the diffused p+ region is not a rectangle, but a circle, which has a radius of curvature and thus cause the pre-breakdown in the junction edge [15], [16]. Therefore, the concept of floating guard ring (FGR) structure is performed to overcome this limitation by providing a p+ region in close to the main junction, surrounding it from all sides but separated from it to share the electric field on the main junction [17]. Currently, some different FGR structures have been come up with, including single FGR [18], double FGRs [19], deep FGR [20], etc. The impact of FGR's size and location have been widely discussed [21], [22], but most of the conclusions are based on the theoretical calculations and simulations, not the experimental verifications. Meanwhile, the APD structures are developing towards smaller sizes. As a result, it is necessary to experimentally study the impact of the size and the location of FGR on small-size APDs' performance.

In this paper, we designed and fabricated sixteen 50 μm photosensitive area planar InP/InGaAs-based SAGCM APD devices with different single FGR structures (size and location), whose dark current was in the nA level. The effects of different FGR structures on the punch-through voltage and breakdown voltage were investigated, which demonstrated that there was an optimal FGR diameter and distance between FGR and the diffused p+ region in APD with a 50 μm photosensitive area. Furthermore, the dark currents, gains and photo responsibility were also measured and discussed, revealing the relatively good performance.

II. Experiments

A. Material Epitaxy

The cross-section diagram of the planar InP/InGaAs-based SAGCM APD device designed in this paper was shown in Fig. 1(a). The epitaxial structure was grown on a 2-inch n-InP substrate by Metal-Organic Chemical Vapor Deposition (MOCVD). Firstly, a 500 nm heavily doped n^+-InP buffer layer was deposited with the concentration of 2×10^{18} cm^{-3} to get a smooth surface. In order to suppress the band difference between n^+-InP/InGaAs heterointerface, an unintentionally doped InP layer with the thickness of 500 nm was epitaxied before a 2.5 μm-thick undoped $In_{0.53}Ga_{0.47}As$ absorption layer. The next layers were a 10 nm-thick, 1×10^{17} cm^{-3}-doped n-InGaAs layer and a 90 nm-thick, 2×10^{16} cm^{-3}-doped n-$In_{0.53}Ga_{0.47}As_yP_{1-y}$ compositionally gradient layer, respectively, which could reduce the valence band difference and hole barrier between the InP/InGaAs interface [23]. Subsequently, a thin and highly doped InP charge layer was sandwiched between the InGaAsP

TABLE I
THE DESIGNED THICKNESS AND CARRIER CONCENTRATION OF EACH LAYER

Layers	Thickness (μm)	Carrier concentration (cm^{-3})
i-InGaAsP (E_g=1.13-1.24eV) contact layer	0.12	<2×10^{15}
i-InP multiplication layer	3.6	<1×10^{16}
n-InP charge layer	0.065	4.8×10^{17}
n-InGaAsP grading layer (E_g=0.83-0.89eV)	0.03	2×10^{16}
n-InGaAsP grading layer (E_g=0.95-1.03eV)	0.03	2×10^{16}
n-InGaAsP grading layer (E_g=1.13-1.24eV)	0.03	2×10^{16}
n-InGaAs grading layer	0.01	1×10^{17}
InGaAs absorption layer	2.5	<5×10^{14}
i-InP	0.5	<2×10^{15}
n-InP buffer layer	0.5	2×10^{18}
n-InP substrate	350	2-8×10^{18}

grading layer and the 3.6 μm-thick undoped i-InP layer, to avoid the high field ionization in the undoped InGaAs absorption layer [24]. The doping concentration and the thickness of the charge layer is 4.8×10^{17} cm^{-3} and 65 nm, respectively. On the top, there was a 120 nm i-$In_{0.53}Ga_{0.47}As_yP_{1-y}$ with the bandgap between 1.13 eV and 1.24 eV to make a better ohmic contact after diffusion. The specific thickness and concentration of each layer are listed in Table I.

B. Device Fabrication

After the wafer epitaxy, the corresponding device fabrication process was shown in Fig. 1(b)–(d). The SiN_x film was grown by ICP-PECVD under a low temperature to regard as the passivation layer and the hard mask of diffusion process at the same time. A first lithography process formed the diffusion trench openings for diffusion regions. Whereafter, part of the SiN_x was etched by RIE technology. The formation of the heavily doped p^+-InP region and the FGR region that suppress edge-breakdown were achieved by single MOCVD diffusion of zinc simultaneously. After that, another thinner SiN_x film was deposited by ICP-PECVD to form the antireflection layer and isolation layer between the p^+-InP and FGR. SiN_x was selectively etched by RIE to exposure partial p^+-InP, for convenience of forming metal contact in the next steps. Then, the top p-electrode and the electrode pad were deposited using electron beam evaporation (EBE) technology in one step. Finally, with the purpose of getting a new, clean and flat back surface, the devices were treated by well-controlled grinding and polishing. The bottom n-electrode was deposited on the treated back surface by EBE in hot pursuit. The ohmic contacts were formed by rapidly annealing in a nitrogen atmosphere.

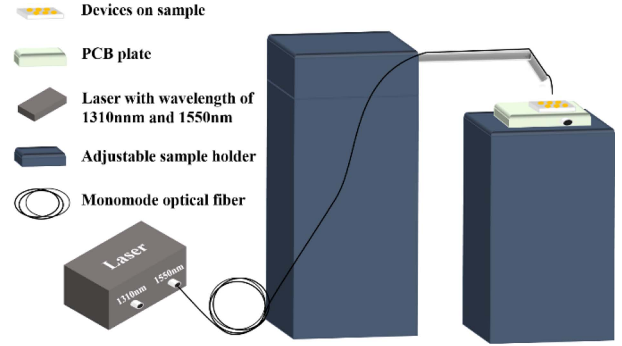

Fig. 2. Schematic diagram of the self-built dark and light current test equipment.

III. CHARACTERZATION

The design of devices and the surface topography were measured by optical microscope (OM). Scanning electron microscope (SEM) technology was carried out to confirm the exact thickness of the diffusion layer. The current-voltage (I-V) characteristic of the devices was measured in dark and light condition by a self-built test equipment and Keithley 4200 semiconductor analyzer (Keithley 4200-SCS), as seen in Fig. 2. To obtain the device responsivity, a monomode optical fiber was setup with laser (1.9 μW, 1550 nm) and the laser spot size on the devices was fixed at 10 μm in diameter. Exposing the devices directly below the optical outlet of the fiber to make sure that the 1550 nm incident light could reach the center of the photosensitive surface of the devices vertically during the I-V test. Subsequently, Keithley 4200-SCS was adopted to obtain the I-V characteristic curves under dark and light condition, respectively. Notice that all the tests in this paper were carried out at room temperature.

IV. RESULTS AND DISCUSSIONS

A. OM and SEM

Fig. 3(a) shows the designed top-view illustration, where L_1 is the diameter of the FGR region, and L_2 is the distance between the diffused p^+ region and FGR, respectively. After the device fabrication, Fig. 3(b) shows the top-view OM image of the 50 μm photosensitive-area APD, while Fig. 3(c) shows the top-view SEM image of the same device. From the Fig. 3(b) and 3(c), it can be seen that the L_1 values are 4.29 μm and 4.39 μm, respectively; while the L_2 values are 3.51 μm and 3.54 μm, respectively. The experimental values of L_1, L_2 are roughly consistent with the designed value 4 μm. L_1 is slightly larger than the design value, while L_2 is slightly smaller, which benefits from the existence of lateral diffusion during the diffusion process.

The top-view and cross-sectional SEM images are performed to analyze the distance, thickness, and diffusion depth, as shown in Fig. 4(a)–(c). And for convenience, the rule of numbering of devices is based on (photosensitive diameter in μm, L_1 (μm)- L_2

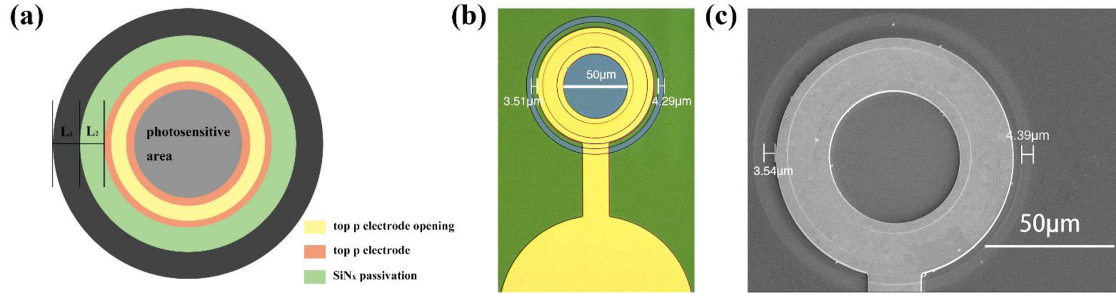

Fig. 3. (a) The specific definition diagram of the photosensitive area, L_1 and L_2; (b) the enlarged top-view OM image and (c) the enlarged top-view SEM image of the 50 μm photosensitive area APD device.

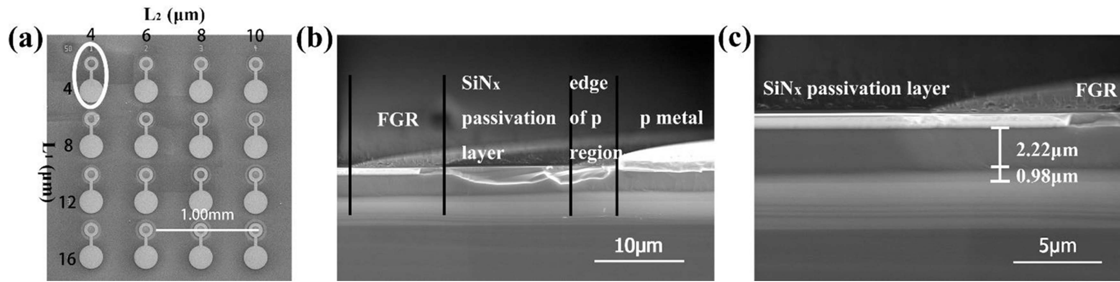

Fig. 4. (a) The top-view of SEM image of the devices with 50 μm photosensitive area; (b) the cross-section diagram of a 50 μm photosensitive area APD device; (c) the cross-section image of the L_2-region of a 50 μm photosensitive area APD device.

(μm)) in this paper. For instance, the device circled in Fig. 4(a) is named (50, 4–4). Fig. 4(b) is the cross-section diagram contains both the L_1-region and the L_2-region of a 50 μm photosensitive area APD device. While Fig. 4(c) is the cross-section image of the L_1-region of the same APD device with a larger magnification. In Fig. 4(b), both in the edge of FGR and the edge of p^+ region, the curved edges can be seen clearly, implying that the measured thickness of the diffused p+-InP layer is 2.22 μm. Considering the unexpected inclination of samples and the rough cleavage cross-section, the actual thickness is slightly larger than above value, which roughly meets our design and accordance with other studies [25], [26].

B. I-V Characteristics

The key parameters, such as the punch-through voltage (V_{pt}), breakdown voltage (V_{br}), dark current (I_d), etc., are extracted from the *I-V* curves directly. Following are the definitions of above parameters:

1. Punch-through Voltage (V_{pt}): the reverse voltage applied on the devices when the depletion region diffuses into InGaAs absorption layer.
2. Breakdown Voltage (V_{br}): because the magnitude of dark current before breakdown is nA, the V_{br} is defined as the bias voltage when the dark current reaches 1 μA [27].
3. Dark Current (I_d): the current when the bias voltage is equal to 0.95 V_{br} under the dark condition.
4. Light Current (I_L): the current when the bias voltage is equal to 0.95 V_{br} under the light condition.
5. Photocurrent (I_p): the difference between the I_L and I_d, namely $I_p = I_L - I_d$.

All the APDs exhibit typical *I-V* characteristics, and the *I-V* curve under the dark and light condition for the sample (50, 12–8) is plotted in Fig. 5(a). From the *I-V* plot, the V_{pt}, V_{br}, I_d and I_L, can be extracted, and their values are 14.6 V, 32.7 V, 1.1 nA and 3.9 μA, respectively. Similarly, above parameters for all the samples could be extracted and plotted in Fig. 5(b)–(d).

Fig. 5(c) shows that the dark currents of all devices are on the level of nA. The relationship between the V_{br} and L_1, L_2 of the 50 μm photosensitive area samples is plotted in Fig. 5(b), and the V_{br} values for all devices are around 35 V, which means the effect of L_1 and L_2 on the V_{br} is weak. Fig. 5(b) also shows the relationship between the V_{pt} and L_1 and L_2, and it can be seen surprisingly that every time L_1 and L_2 vary, the punch-through voltage varies a lot, which can reveal the suppression of edge breakdown to some extent. As we know, when the depletion region reaches InGaAs absorption layer, the APD device begins to punch through, and the photogenerated carriers in the absorption layer start to conduct as a photocurrent [28], [29]. By solving the Poisson equation, the ideal expression of the punch-through voltage is [29]:

$$V_{pt} = \frac{qN_m}{2\epsilon_{InP}\epsilon_0} d_{em}^2 + \frac{1}{2}(2d_{em} + d_c)\frac{qN_c}{2\epsilon_{InP}\epsilon_0} d_c + \frac{1}{2}(2d_{em} + 2d_c + d_g)\frac{qN_g}{2\epsilon_{InGaAsP}\epsilon_0} d_g. \quad (1)$$

Where, N_m, d_{em} is the carrier concentration and efficient thickness of i-InP multiplication layer, respectively; N_c, d_c is the carrier concentration and thickness of n-InP charge layer, respectively; N_g, d_g is the carrier concentration and the thickness of n-InGaAsP grading layer, respectively; $\epsilon_{InP} = 12.5$ is the relative

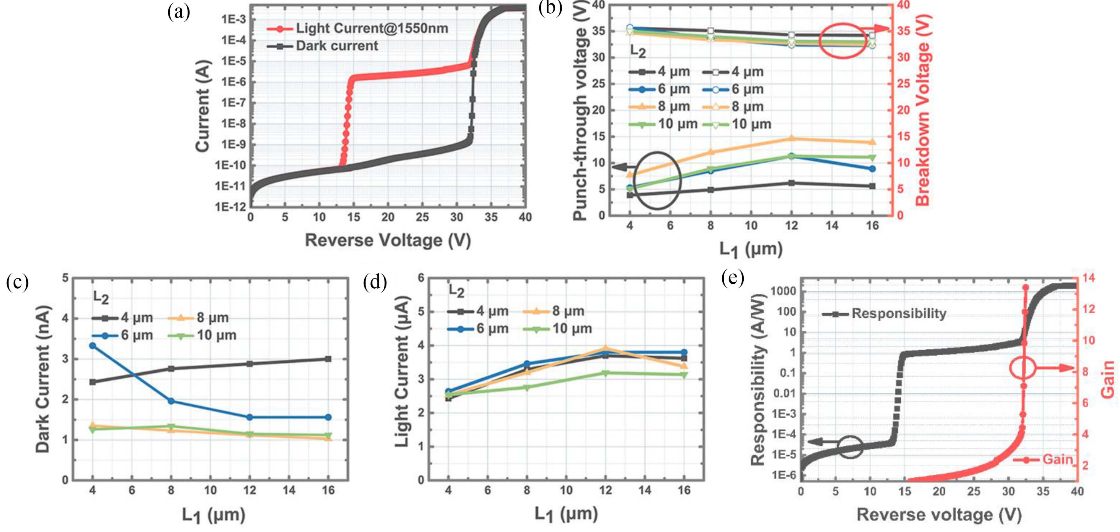

Fig. 5. (a) The *I-V* characteristic curve of the (50, 12–8) device; (b) the diagram of the punch-through voltage (V_{pt}) and breakdown voltage (V_{br}); (c) the dark current curves; (d) the light current curves of the 50 μm photosensitive area samples; (e) the *M-V* and $\mathcal{R}$-*V* characteristic curves of the (50, 12–8) device (The trend line is just guide of eyes).

dielectric constant of InP; $\epsilon_{InGaAs_{1-y}P_y} = 12.5 + 1.44y$ is the relative dielectric constant of $InGaAs_{1-y}P_y$; $\epsilon_0 = 8.85 \times 10^{-12}$ F/cm is the dielectric constant of vacuum.

Based on (1), it is clear that the larger the d_m is, the larger the V_{pt} is. And d_{em} satisfies the following formula:

$$d_{em} = d_m - W. \tag{2}$$

Where, d_m is the designed thickness of i-InP, $W = \sqrt{\frac{2\epsilon_{InP} E_m}{N_p}}$ is the depletion width of p-i InP junction [30]. Hence, the higher the maximum electric field E_m is, the smaller the d_{em} is, which means the higher punch-through voltage represents the lower E_m, and thus represents the weaker edge field. From all above results and discussions, it can be concluded that the optimized values of L_1 and L_2 for the 50 μm photosensitive area APDs are 12 μm and 8 μm, respectively.

The principle of the FGR structure that can prevent edge breakdown is that the junction between the heavily doping FGR and multiplication i-region can share and reduce the potential drop on the main junction to some extent [16]. With L_1 and L_2 increasing, the efficiency junction area of APD gradually increases, because the junction of p^+-InP is overlapped with that of FGR in both sides. But if L_2 reaches a critical value (8 μm in this paper) when the depletion region of the p^+ junction and FGR separate in spatial terms, the FGR deservedly doesn't make sense. Therefore, there is a trade-off value for L_1 and L_2, and thus a high-performance APD device can be obtained.

Furthermore, the gain and the responsibility of (50, 12–8) device are also investigated. The gain-voltage (*M-V*) curves and responsibility-voltage ($\mathcal{R}$-*V*) curves are shown in Fig.5(e). Defining that the voltage for unity gain $V(M = 1)$ is the voltage where the second derivative of the photo current with respect to the voltage $\partial^2 Ip/\partial V^2$ tends to zero [31]. Usually, the formula to calculate gain (*M*) is simplified as [4], [32]:

$$M(V) = \frac{I_L(V) - I_d(V)}{I_L(M=1) - I_d(M=1)} \tag{3}$$

Where, $I_L(V)$ and $I_d(V)$ is the light current and dark current under reverse bias voltage, respectively. $I_L(M = 1)$ and $I_d(M = 1)$ is the light current and dark current when $M = 1$. The gain can be up to 10 until the device breaks down. The lower gain in this paper is mainly attributed to the design of our epitaxial structure [26], [33], which we are going to improve in the future. Also, the devices' responsibility at $M = 10$ is calculated as following [34], [35]:

$$\mathcal{R} = \frac{I_p}{P_{in}} = \frac{\eta q \lambda}{hc} M. \tag{4}$$

Where, $I_p = I_L - I_d$, is the photocurrent; $P_{in} = 1.9\ \mu$W, is the incident light power, *h* is the Plank constant, $\lambda = 1550$ nm is the wavelength of the incident light, *c* is the speed of light in vacuum, and η is the symbol of quantum efficiency. The $\mathcal{R}$ and η of (50, 12–8) device is calculated to be about 9.01 A/W when $M = 10$ and 72%, respectively.

V. Conclusion

In conclusion, the planar SAGCM APDs with kinds of FGRs are fabricated and characterized with 50 μm photosensitive area in this paper. Comparing the breakdown voltage and punch-through voltage of these devices, there are optimal target values for the FGR parameters L_1 and L_2, which result in the best suppression of the pre-breakdown in the edge junction. The optimized parameters and related device with relatively low dark current (nA-level), high responsibility (9.01 A/W at $M = 10$), high quantum efficiency (72%) and pre-breakdown suppression, can guide future design to improve APDs' performance. However, our epitaxial structure still needs to be ameliorated. More information about these APD devices' noise and dynamic

characteristics also needs further study. And thus, it could be expected to be applied in the short-wave optical communication system.

References

[1] M. H. Mun *et al.*, "Design and simulation result of n substrate reverse type avalanche photodiode (APD)," *IEEE Trans. Nucl. Sci.,* vol. 56, no. 3, pp. 1046–1050, Jun. 2009, doi: 10.1109/TNS.2008.2012258.

[2] O. Kharraz and D. Forsyth, "Performance comparisons between PIN and APD photodetectors for use in optical communication systems," *Optik,* vol. 124, no. 13, pp. 1493–1498, 2013, doi: 10.1016/j.ijleo.2012.04.008.

[3] O. Kharraz and D. Forsyth, "PIN and APD photodetector efficiencies in the longer wavelength range 1300–1550nm," *Optik,* vol. 124, no. 16, pp. 2574–2576, 2013, doi: 10.1016/j.ijleo.2012.07.035.

[4] A. S. Huntington, "1 - Types of avalanche photodiode," presented at the InGaAs avalanche photodiodes for ranging and lidar," 2020. [Online]. Available: https://www.sciencedirect.com/science/article/pii/B9780081027257000015

[5] S. Cao *et al.*, "Theoretical analysis of InGaAs/InAlAs single-photon avalanche photodiodes," *Nanoscale Res. Lett.,* vol. 14, no. 1, 2019, Art. no. 3, doi: 10.1186/s11671-018-2827-4.

[6] C. Wang *et al.*, "Design considerations of InGaAs/InP single-photon avalanche diode for photon-counting communication," *Optik*, vol. 185, pp. 1134–1145, May 2019, doi: 10.1016/j.ijleo.2019.04.053.

[7] H. Y. Zhao, N. Naseem, A. H. Jones, J. C. Campbell, and J. W. Shi, "High-speed and wide dynamic range avalanche photodiode for coherent lidar application," in *Proc. IEEE Photon. Conf.*, 2019, pp. 1–2.

[8] M. A. Itzler, K. K. Loi, S. Mccoy, N. Codd, and N. Komaba, "High-performance, manufacturable avalanche photodiodes for 10 Gb/s optical receivers," in *Proc. Opt. Fiber Commun. Conf.*, vol. 4, 2000, pp. 126–128.

[9] O. Kharraz and D. Forsyth, "Performance comparisons between PIN and APD photodetectors for use in optical communication systems," *Optik - Int. J. Light Electron Opt.,* vol. 124, no. 13, pp. 1493–1498, 2012.

[10] K. Nishida, K. Taguchi, and Y. Matsumoto, "InGaAsP heterostructure avalanche photodiodes with high avalanche gain," *Appl. Phys. Lett.,* vol. 35, no. 3, pp. 251–253, 1979.

[11] S. R. Forrest, R. F. Leheny, R. E. Nahory, and M. A. Pollack, "$In_{0.53}Ga_{0.47}As$ photodiodes with dark current limited by generation-recombination and tunneling," *Appl. Phys. Lett.,* vol. 37, no. 3, pp. 322–325, 1980.

[12] Y. Takanashi, M. Kawashima, and Y. Horikoshi, "Required donor concentration of epitaxial layers for efficient InGaAsP avalanche photodiodes," *Japanese J. Appl. Phys.,* vol. 19, no. 4, pp. 693–701, 1980, doi: 10.1143/jjap.19.693.

[13] S. R. Forrest, "Optical response time of $In_{0.53}Ga_{0.47}As$/InP avalanche photodiodes," *Appl. Phys. Lett.,* vol. 41, no. 1, pp. 95–98, 1982.

[14] C. P. Skrimshire and J. R. Farr, "Reliability of mesa and planar InGaAs PIN photodiodes," *IEEE Proc. J.,* vol. 137, no. 1, pp. 74–78, 1990.

[15] B. Lee and I. Yun, "Effect of different etching processes on edge breakdown suppression for planar InP/InGaAs avalanche photodiodes," *Microelectronics J.,* vol. 33, no. 8, pp. 645–649, 2002, doi: 10.1016/S0026-2692(02)00032-0.

[16] S. M. Sze and G. Gibbons, "Effect of junction curvature on breakdown voltage in semiconductors," *Solid State Electron.,* vol. 9, no. 9, pp. 831–845, 1966.

[17] V. Mishra, V. D. Srivastava, and S. K. Kataria, "Role of guard rings in improving the performance of silicon detectors," *Pramana,* vol. 65, no. 2, pp. 259–272, 2005.

[18] M. S. Adler, V. Temple, A. P. Ferro, and R. C. Rustay, "Theory and breakdown voltage for planar devices with a single field limiting ring," *IEEE Trans. Electron Devices,* vol. 24, no. 2, pp. 107–113, Feb. 1977.

[19] D. E. Ackley and J. Hladky, "In/sub 0.53/Ga/sub 0.47/As/InP floating guard ring avalanche photodiodes fabricated by double diffusion," *IEEE Photon. Technol. Lett.,* vol. 2, no. 8, pp. 571–573, Aug. 1990.

[20] K. Hyun, Y. Paek, Y. Kwon, S. Hwang, J. Shim, and S. Ahn, "Pre-breakdown suppression in planar InP/InGaAs avalanche photodiode using deep floating guard ring," *Appl. Phys. Lett.,* vol. 85, no. 23, pp. 5547–5549, 2004.

[21] V. Mishra *et al.*, "Studies on reducing leakage current and improving breakdown voltage of large-area silicon detectors: Technology and results," *Nucl. Inst. Methods Phys. Res. A,* vol. 527, no. 3, pp. 308–318, 2004.

[22] S. H. Park, C. Y. Park, and D. Ahn, "Simulation studies on guard ring effects on edge breakdown suppression of InGaAs/InP avalanche photodiodes," *Japanese J. Appl. Phys.,* vol. 57, no. 10, pp. 106506.1–106506.3, 2018.

[23] Y. Matsushima, S. Akiba, K. Sakai, Y. Kushiro, Y. Noda, and K. Utaka, "High-speed-response InGaAs/InP heterostructure avalanche photodiode with InGaAsP buffer layers," *Electron. Lett.,* vol. 18, no. 22, 1982, Art. no. 945.

[24] L. E. Tarof and J. Yu, "High-frequency performance of separate absorption grading, charge, and multiplication InP/InGaAs avalanche photodiodes," *IEEE Photon. Technol. Lett.,* vol. 5, no. 6, pp. 672–674, Jun. 1993.

[25] H. Xing, J. Zhang, A. Liu, and Y. Yang, "Design of high linearity InGaAs/InP avalanche photodiode with a hybrid absorption layer structure," *Infrared Phys. Technol.,* vol. 102, 2019, Art. no. 103018, doi: 10.1016/j.infrared.2019.103018.

[26] Y. Zhao, "Impact ionization in absorption, grading, charge, and multiplication layers of InP/InGaAs SAGCM APDs with a thick charge layer," *IEEE Trans. Electron Devices,* vol. 60, no. 10, pp. 3493–3499, Oct. 2013, doi: 10.1109/TED.2013.2279299.

[27] T. Maruyama, "Development of a near-infrared photon-counting system using an InGaAs avalanche photodiode," *Opt. Eng.,* vol. 41, no. 2, 2002, Art. no. 395.

[28] P. A. Hiskett *et al.*, "Performance and design of InGaAs/InP photodiodes for single-photon counting at 1.55 μm," *Appl. Opt.,* vol. 39, no. 36, pp. 6818–6829, 2000, doi: 10.1364/AO.39.006818.

[29] K. S. Hyun and C. Y. Park, "Breakdown characteristics in InP/InGaAs avalanche photodiode with p-i-n multiplication layer structure," *J. Appl. Phys.,* vol. 81, no. 2, pp. 974–984, 1997.

[30] S. M. Sze, *Physics of Semiconductor Devices*, 2nd ed. Hoboken, NJ, USA: Wiley, 1981.

[31] H. T. J. Meier, "Design, characterization and simulation of avalanche photodiodes," *ETH*, 2011, doi: 10.3929/ethz-a-006445001.

[32] R. J. Mcintyre, "Multiplication noise in uniform avalanche diodes," *IEEE Trans. Electron Devices,* vol. ED-13, no. 1, pp. 164–168, Jan. 1966.

[33] S. Cao *et al.*, "Theoretical studies on InGaAs/InAlAs SAGCM avalanche photodiodes," *Nanoscale Res. Lett.,* vol. 13, 2018, Art. no. 158.

[34] A. Rogalski, *Infrared Detectors*, 2nd ed. Boca Raton, FL, USA: CRC Press, 2010, pp. 45–74.

[35] K. A. S. Al-Khateeb, N. S. Nafi, and K. Hasan, "Design and characterization of single photon APD detector for QKD application," in *Proc. Int. Conf. Comput. Commun. Eng.*, 2010, pp. 1–5, doi: 10.1109/ICCCE.2010.5556839.